environments

Article

Late 20th Century Hypereutrophication of Northern Alberta's Utikuma Lake

Carling R. Walsh [1,*], Fabian Grey [2], R. Timothy Patterson [1], Maxim Ralchenko [1], Calder W. Patterson [3], Eduard G. Reinhardt [4], Dennis Grey [2], Henry Grey [2] and Dwayne Thunder [2]

[1] Ottawa-Carleton Geoscience Centre Department of Earth Sciences, Carleton University, Ottawa, ON K1S 5B6, Canada
[2] Whitefish Lake First Nation #459, General Delivery, Atikameg, AB T0G 0C0, Canada
[3] Solstice Environmental Management, 10714 176 Street NW, Edmonton, AB T5S 1G7, Canada
[4] School of Earth, Environment, and Society, McMaster University, Hamilton, ON L8S 4L8, Canada
* Correspondence: carling.walsh@carleton.ca

Abstract: Eutrophication in Canadian lakes degrades water quality, disrupts ecosystems, and poses health risks due to potential development of harmful algal blooms. It also economically impacts the general public, industries like recreational and commercial fishing, and tourism. Analysis of a 140-year core record from Utikuma Lake, northern Alberta, revealed the processes behind the lake's current hypereutrophic conditions. End-member modeling analysis (EMMA) of the sediment grain size data identified catchment runoff linked to specific sedimentological processes. ITRAX X-ray fluorescence (XRF) elements/ratios were analyzed to assess changes in precipitation, weathering, and catchment runoff and to document changes in lake productivity over time. Five end members (EMs) were identified and linked to five distinct erosional and sedimentary processes, including moderate and severe precipitation events, warm and cool spring freshet, and anthropogenic catchment disturbances. Cluster analysis of EMMA and XRF data identified five distinct depositional periods from the late 19th century to the present, distinguished by characteristic rates of productivity, rainfall, weathering, and runoff linked to natural and anthropogenic drivers. The most significant transition in the record occurred in 1996, marked by an abrupt increase in both biological productivity and catchment runoff, leading to the hypereutrophic conditions that persist to the present. This limnological shift was primarily triggered by a sudden discharge from a decommissioned sewage treatment lagoon into the lake. Spectral and wavelet analysis confirmed the influence of the Arctic Oscillation, El Niño Southern Oscillation, North Atlantic Oscillation, and Pacific Decadal Oscillation on runoff processes in Utikuma Lake's catchment.

Keywords: eutrophication; end member modeling analysis; ITRAX-XRF; paleolimnology; time series analysis

Academic Editor: Peiyue Li

Received: 19 December 2024
Revised: 4 February 2025
Accepted: 8 February 2025
Published: 11 February 2025

Citation: Walsh, C.R.; Grey, F.; Patterson, R.T.; Ralchenko, M.; Patterson, C.W.; Reinhardt, E.G.; Grey, D.; Grey, H.; Thunder, D. Late 20th Century Hypereutrophication of Northern Alberta's Utikuma Lake. *Environments* **2025**, *12*, 63. https://doi.org/10.3390/environments12020063

1. Introduction

Many First Nations communities across Canada rely on their culturally important traditional lands, and particularly the aquatic ecosystem services derived from wetlands, lakes, and streams. For the members of Treaty 8 White Fish Lake First Nation #459 (WLFN, Atikameg; Figure 1), the whitefish (*Coregonus clupeaformis*) populations in Utikuma Lake have been a vital source of sustenance for generations and have supported the local economy since the establishment of a commercial fishery in the 1940s. However, there has been a significant decline in the whitefish population in recent years as Utikuma Lake

became increasingly eutrophic, and at present has reached hypereutrophic status with cyanobacteria blooms observed [1]. The acceleration of eutrophication starting in the mid-1990s eventually rendered the lake's whitefish fishery financially unsustainable, causing negative impacts on the community. By 2012, the fishery had completely collapsed (Fabian Grey, Pers. Comm., 2024). In an effort to determine whether there had been any recovery in the whitefish population, netting sessions lasting 16 and 24 h, respectively, during summer 2023, were attempted but yielded no fish (Dwayne Thunder, Pers. Comm., 2023).

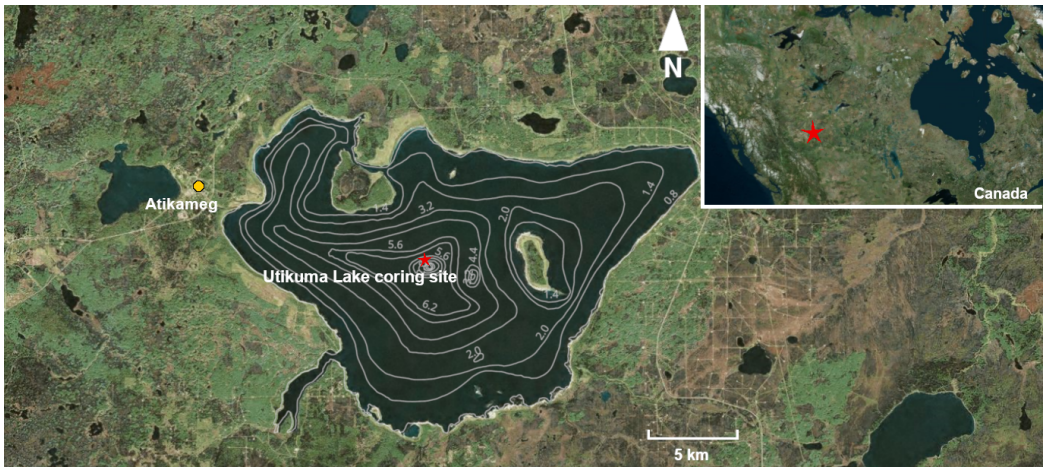

Figure 1. Map showing Utikuma Lake, its location within Canada (star, upper right inset), as well as the location of the community of Atikameg (Whitefish Lake First Nation #459) on the western shore. The coring site is indicated by a red star, at which four closely spaced gravity cores were collected. Location and core details are presented in Table 1. Bathymetric contours are given in meters.

Table 1. Sediment coring stations and details for each collected core.

Utikuma Lake		
Date Collected:	16 June 2022	
Sampling Location:	55.86914508, −115.42383901	
Sampling Depth (m):	4.5	
Core ID	**Core Length (mm)**	**Sampling Resolution (mm)**
BU1	459	1
BU2	355	1
BU3	345	5
BU4	370	5

While the primary causes of eutrophication are unclear, community elders and knowledge keepers implicate documented large scale sewage releases from two upstream decommissioned sewage treatment lagoons as potential contributors—one incident in 1996 and the second in 2004. There is also the possibility that climate variability or other types of land use change accompanying the well-documented mid-20th century Great Acceleration may have also been contributing to the observed degradation and the development of harmful algal blooms in the lake [2,3]. The decline in water quality and the rising frequency of algal and cyanobacterial blooms has been observed in lakes throughout the region and worldwide, presenting an emergent and persistent environmental challenge [4–10]. Understanding the relationship between anthropogenic and natural drivers of eutrophication may help to inform management and remediation strategies of lakes worldwide.

Retrospective long-term proxy records of past environmental conditions are necessary to place current conditions into context [11]. Freshwater lakes archive continuous sedimentary records of biological, chemical, and physical proxies of past environmental conditions, influenced by broad-scale patterns of natural climate variability and anthropogenic disturbances [12–14].

The purpose of this study was to evaluate potential natural and human-induced factors influencing the environmental conditions and eutrophication trajectory of Utikuma Lake from the late 19th century to present. With the support of members of WLFN, gravity cores were collected from Utikuma Lake for paleolimnological analyses, including ITRAX-XRF core scanning and grain size analysis. These analyses were selected to give insights into the nature and timing of physical and chemical changes that have occurred in the lake and correlate observed paleolimnological changes to known climatic and/or anthropogenic influences.

Study Area

Utikuma Lake (Figure 1), a large, shallow lake covering 288 km^2, lies at an elevation of 648 m. It is situated within the Peace River drainage basin in northwestern Alberta, approximately 65 km northeast of High Prairie, Alberta. The lake is bordered by the Gift Lake Métis settlement on the western shore and the 8300 ha WLFN on the norethern and western shore. Much of the shoreline is relatively undeveloped, save for the community of Atikameg, the WLFN headquarters (population 880, Statistics Canada 2021 census). Characterized by a single basin, Utikuma Lake has a maximum depth of 5.5 m and an average depth of 1.7 m [15].

Utikuma Lake is fed by a catchment area that covers around 2170 km^2. The ratio of the watershed area to the lake area is approximately 7.5:1, which is relatively small compared to most lakes in Alberta, suggesting lower than average surface water flow into the lake. The lake receives water from several surface inflows, including the Utikuma River, which brings water from Utikumasis Lake (situated 3 km west of Utikuma Lake), along with several unnamed permanent streams with a variety of origins. The main outflow from Utikuma Lake is the continuation of the Utikuma River on the north shore, which eventually merges with the Muskwa, Wabasca, and Peace Rivers [15,16]. The Utikuma Lake catchment area is in the Central Mixed Wood subregion of the Boreal Forest Natural Region of Alberta in an area comprised of generally rolling topography overlain by mixed boreal forest and wetlands [17]. The underlying substrate includes a variety of Cretaceous sedimentary rocks that host rich petroleum reserves.

The climate is continental, characterized by cold, long winters and short, cool summers. Based on the 1971–2000 climate normals, which describe the average climatic conditions from the nearest year-round meteorological recording station at Slave Lake (55°18′ N, 114°46′ W), located approximately 65 km to the southeast, the average annual temperature is 1.7 °C. Monthly temperatures average from −13.5 °C in January to 16.4 °C in July [18]. The average annual precipitation is 422 mm, with 70% occurring as rain from May to September. The highest average daily precipitation, around 2.4 mm per day, is recorded between early June and mid-July, followed by a relatively drier period from mid-July to the end of August, with approximately 2.0 mm per day [18].

2. Materials and Methods

2.1. Core Collection and Subsampling

Both UWITEC and Glew-type sediment corers were deployed to collect gravity cores from Utikuma Lake (55.86914508° N, −115.42383901° W) from a boat supplied by D. Thunder of WLFN (Figures 1 and 2A, Table 1). Four closely spaced cores were collected from Utikuma Lake (designated BU1–4) from a water depth of 4.5 m. As the collected cores were composed of very soft sediments, they were kept upright during transport to shore to avoid homogenization of the sediment and were either subsampled in the field, or in nearby High Prairie, AB, at 1 mm or 5 mm resolutions using a portable custom designed high-resolution extruder (Figure 2B,C, Table 1; [19]). Each core was completely subsampled and kept refrigerated during transport to Carleton University, where they were stored under refrigeration prior to subsequent analyses.

Figure 2. Photographs showing (**A**) collection of a UWITEC gravity core from Utikuma Lake as the bottom of the core is capped upon recovery, (**B**) a UWITEC core barrel filled with a core mounted on a custom-built portable extruder that can be deployed in the field and which can produce 1 mm resolution subsamples, and (**C**) a 1 mm resolution subsample being transferred from the extruder into a sample bag for subsequent analysis.

2.2. ^{210}Pb Chronology

Select 5 mm resolution samples from core BU4 were sent to the Blais Radioisotope lab at the University of Ottawa for ^{210}Pb dating. ^{210}Pb is a radionuclide in the ^{238}U decay chain, with a half life of approximately 22 years. The ^{210}Pb activity was measured for each sample (in Bq/kg) using a gamma spectrometer [20]. Corresponding dates of deposition of the bottom of each sample interval were calculated from the resulting activity measurements using the following formula:

$$Date = sampling\ date - \left(\frac{1}{\lambda}\right) ln\left[\frac{A_0}{A_x}\right] \quad (1)$$

where λ is the decay constant of ^{210}Pb (0.03114 year^{-1}), A_0 is the total ^{210}Pb activity for the sediment core, and A_x is the cumulative ^{210}Pb activity at the given depth x [20]. Results of the gamma spectrometry are presented in Table 2. A spline interpolation was fitted to the age-depth values, which was then used to extract dates at the 1 mm resolution to be used in subsequent analyses (Figure 3).

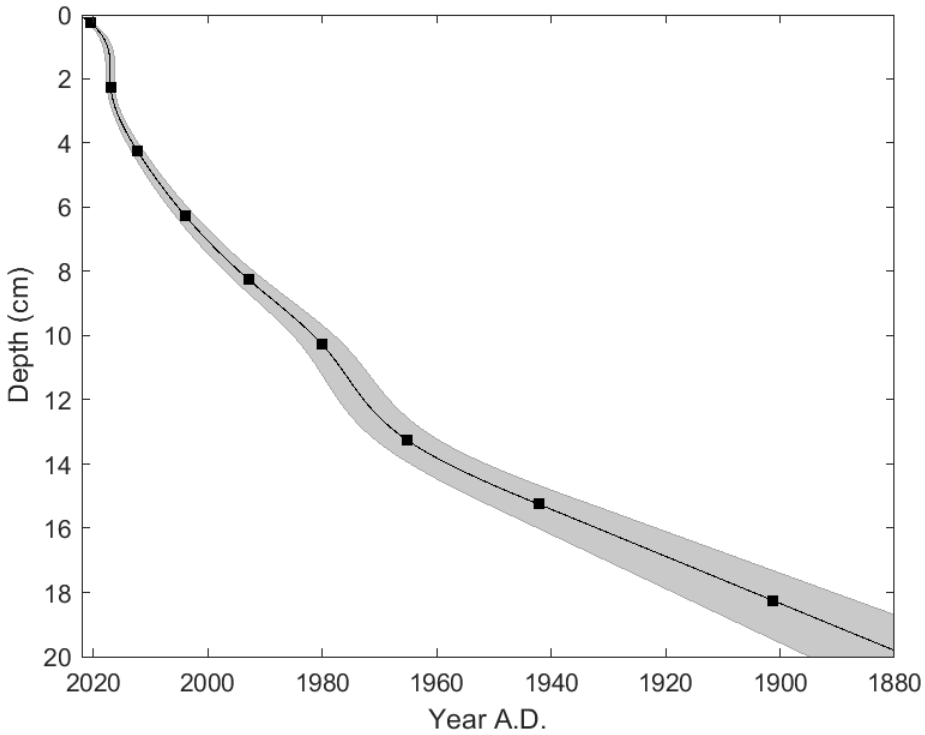

Figure 3. ^{210}Pb age model (black) and standard deviation (grey) for Utikuma Lake, with an average sedimentation rate of 1.5 mm/yr.

Table 2. ^{210}Pb activity and calculated dates by sample for Utikuma Lake Core BU4. Activity below 185 mm was below the detection limit.

Utikuma Lake (BU4)					
Depth (mm)	**^{210}Pb Total Activity (Bq/kg)**	**^{210}Pb Activity Error (Bq/kg)**	**Age (Years BP)**	**Age Error (Years)**	**Average Date of Deposition (Years AD)**
0-5	330.26	44.84	1.97	0.34	2020.48
20–25	238.41	29.81	5.52	0.64	2016.94
40–45	296.85	34.72	10.22	1.08	2012.23
60–65	264.15	31.26	18.49	1.74	2003.97
80–85	217.27	31.66	29.62	2.65	1992.83
100–105	224.98	33.73	42.35	3.74	1980.10
130–135	181.13	31.75	57.28	5.51	1965.17
150–155	141.47	31.44	80.32	9.01	1942.14
180–185	109.95	33.83	121.20	14.39	1901.25

2.3. ITRAX-XRF Analysis

The upper 200 subsamples at 1 mm resolution from the Utikuma Lake Core BU1 were loaded into sequential sediment reservoir (SSR) vessels and compacted to ensure that there were no void spaces [21]. Only the upper 200 mm of the BU1 core was analyzed as this interval covers the time period of interest prior to the establishment of the commercial fishery to the post-fishery hypereutrophy. The SSRs were stepwise analyzed at 0.2 mm resolution on a Cox ITRAX μXRF-CS using the Mo XRF tube. The resulting elemental data, in counts per second, were normalized against the Mo inc/Mo Coh scattering ratio [22–24]. Two groups of data were used for further analysis. For example, runoff/precipitation were inferred from the Fe, Ti, K/Rb ratio, or Ca/Sr ratio, and productivity were inferred from P, S, and the Si/Ti ratio (Table 3; [11,22,25–27]).

Table 3. Overview of ITRAX elements and elemental ratios used as proxies throughout this study. Note: several of these elements/ratios have been reported as proxies for multiple environmental processes; only those relevant to this study are listed.

Element or Elemental Ratio	Proxy for:	References
Ti	Terrigenous/detrital sediment; runoff	[28]
Fe	Terrigenous/detrital sediment; runoff	[28]
K/Rb	Detrital clay	[22]
Ca/Sr	Detrital carbonate	[28]
P	Primary productivity	[11]
S	Organics; Organic matter decay	[22,27]
Si/Ti	Biogenic silica content	[28]

2.4. Grain Size Analysis

The upper 200 1 mm resolution subsamples of the core BU1 were used for particle size analysis. The subsamples were subjected to a three-step digestion protocol to remove carbonate material, organic matter, and biogenic silica, modified from Murray [29] and van Hengstum et al. [30]. This digestion protocol is as follows:

1. Addition of 10% HCl to dissolve and remove carbonate minerals.
2. Addition of 30% H_2O_2 to oxidize and remove organic matter.
3. Addition of 0.2 M NaOH to dissolve and remove biogenic silica.

The completion of this digestion protocol leaves only silicate material from inorganic sources; thus, the grain size distribution indicates only physical runoff characteristics of the lake catchment.

Following the digestion protocol, the subsamples were analyzed using a Beckman Coulter (Los Angeles, California, USA) LS 13 320 laser diffraction particle size analyzer equipped with a universal liquid module. Subsamples were pipetted into the analyzer until an obscuration to 10 ± 2% was achieved. Each subsample was analyzed in triplicate for its grain size distribution ranging from 0.37 µm to 2000 µm. The triplicates were then averaged for each subsample.

End-Member Modeling Analysis

The averaged grain size distributions for each of the 200 subsamples described above were used for end-member modeling analysis (EMMA). The purpose of EMMA is to characterize the primary grain size distributions (i.e., the end members) within a sediment horizon, which provides information on the depositional regimes within a lake. EMMA was carried out in R (version 4.2.2, [31]) using the package EMMAgeo v.0.9.7 by Dietze and Dietze [32]. Only robust end members (EMs) were included, defined as those with distinct, interpretable loadings that did not overlap, as well as those where similar loadings were consistently observed across most model runs [33].

2.5. CONISS Cluster Analysis of ITRAX Elemental Profiles and EMMA Data

Stratigraphically constrained incremental sum of squares hierarchical clustering (CONISS, [34]) was carried out using the R package "rioja" (v.1.0-5, [35]) to visually identify stratigraphic groupings within the ITRAX elemental profiles and EMMA data. The groupings, or "zones", for the core are specified in Table 4. As this method maintains the stratigraphy of the samples, it allows for the recognition of temporal shifts in the environment—in this case, shifts in lake productivity and runoff characteristics.

Table 4. CONISS cluster results for the combined EMMA and ITRAX elemental profiles of Utikuma Lake Core BU1.

Utikuma Lake (BU1)		
CONISS Group	**Date Range (Years A.D.)**	**Depth (mm)**
Zone 1	pre-1950	144–200
Zone 2	1950–1973	115–144
Zone 3	1973–1996	79–115
Zone 4	1996–2017	18–79
Zone 5	2017–present	0–18

2.6. Time Series Analysis

Prior to applying time series analysis transformations, the ITRAX and EMMA data were resampled alongside the ^{210}Pb age model to produce evenly spaced time series for the BU1 core profiles—a requirement for most time series transformations. Blackman–Harris window functions were applied to the resampled data to reduce spectral leakage, and the windowed time series were then filtered to remove low-frequency signals [36].

Spectral and wavelet analysis was carried out on the treated ITRAX and EMMA time series for core BU1. Each of these analyses transform time series data into their frequency-domain counterpart. Thomson's Multitaper Method (MTM, [37]) was used to carry out the spectral analysis transforms. This method compares a series of sinusoidal waveforms of varying frequencies to the input data (here, the ITRAX/EMMA time series) to assess its frequency content. Waveforms with a high incidence with the input data are represented as high "power" at the respective frequency on the resulting periodogram. The MTM is a unique method of this transformation in that it averages many iterations of this process to eliminate potential biases that may arise when applying just one transformation. The resulting periodograms from this spectral analysis technique provide discrete peaks in the frequency data, allowing for simple interpretation. Monte Carlo and chi-square methods were used to estimate red noise and confidence levels, respectively [38,39].

Continuous wavelet transforms (CWTs) were used in addition to the MTM to provide information about time-frequency variation. CWTs employ the same fundamentals as the MTM, though using a wavelet instead of a sinusoidal waveform. Furthermore, the MTM is a frequency-only transformation which assumes stationarity in the input data. CWTs do not rely on this assumption, instead comparing the wavelet to the input data stepwise through time, which results in a time-varying frequency transformation. Unlike the MTM, CWTs do not provide discrete peaks. Due to the complementary nature between the two transformations, these techniques are often used in tandem, though results can be marginally different between the two because of differences in their methods [40,41].

3. Results

3.1. Grain Size Analysis

Grain size analysis of core BU1 revealed a clayey silt-dominated sediment distribution in Utikuma Lake (average 71% silt, 25% clay). Five EMs were recognized from the grain size distributions in an EMMA model that explained 76% of total variance (Figure 4). The clay EM01 (mode = 1 µm, 25% of variance explained) is primarily present between 0 and 120 mm. EM02 (mode = 9 µm, 17% of variance explained) and EM03 (mode = 44 µm, 48% of variance explained) are generally dominant throughout the core, though EM03 briefly disappears from the EM distribution between ~27 and 45 mm. EM04 (primary mode = 84 µm, secondary mode = 42 µm, 7.1% of variance explained) and EM05 (mode = 146 µm, 2.9% of variance explained) are sparse throughout the core.

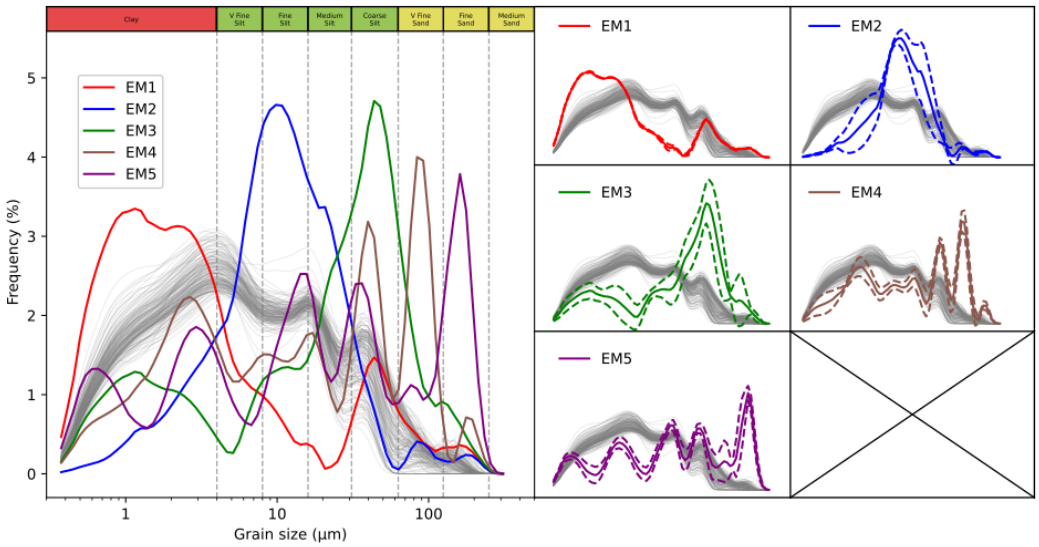

Figure 4. Utikuma Lake Core BU1 grain size frequency distributions for the 200 subsamples (gray plots), as well as the distribution of five robust end members (EMs) derived from the model that best explains the sediment grain size distributions.

3.2. CONISS Clustering of ITRAX and EMMA

The down core profiles of EMMA and ITRAX results in Utikuma Lake were defined by five stratigraphic clusters (Figure 5, Table 4). Zone 1 (pre-1950) elemental profiles of Utikuma Lake is characterized by stability in EM02 and EM03, which are the most dominant EMs in this interval. Runoff proxies—particularly Ti and Fe—are also fairly constant, as are the productivity proxies. Zone 2 (1950–1973) marks a transition, during which EM02 and EM03 remain stable and dominant, but Ti and Fe are reduced, whereas K/Rb and Ca/Sr exhibit sharp aberrations. Within Zone 3 (1973–1996), the distribution of EMs shifted compared to down core; EM02 remained constant, but EM03 decreased. The decrease in EM03 was mirrored by an increase in EM01. Ti and Fe fluctuate regularly during this interval, whereas K/Rb and Ca/Sr are relatively low. The Si/Ti ratio and S values are also relatively low in much of Zone 3 compared to Zones 1 and 2.

Zone 4 (1996–2017) is marked by a strong transition in both runoff and productivity. Ti, Fe, Si, P, and S all show distinct increases at the boundary between Zones 3 and 4 and remain high throughout Zone 4. EMs also show significant changes in this zone. EM02 remains fairly constant, but EM03 fluctuates dramatically until it disappears entirely (∼27–45 mm, 2010–2015). EM01 also becomes more prevalent throughout this zone.

Finally, Zone 5 (2017–present) exhibits a reversal of many of the patterns recognized in Zone 4. After a final peak at the boundary of Zones 4 and 5, the productivity proxies decrease, as do Ti and Fe. EM01 decreased relative to Zone 4, and EM03 is present again. EM04, which was generally low or absent down core, also increases in this zone. Similarly, EM05, which was rare down core, exhibits two aberrations near the top of the core: once just below the Zone 4/5 boundary and once just above.

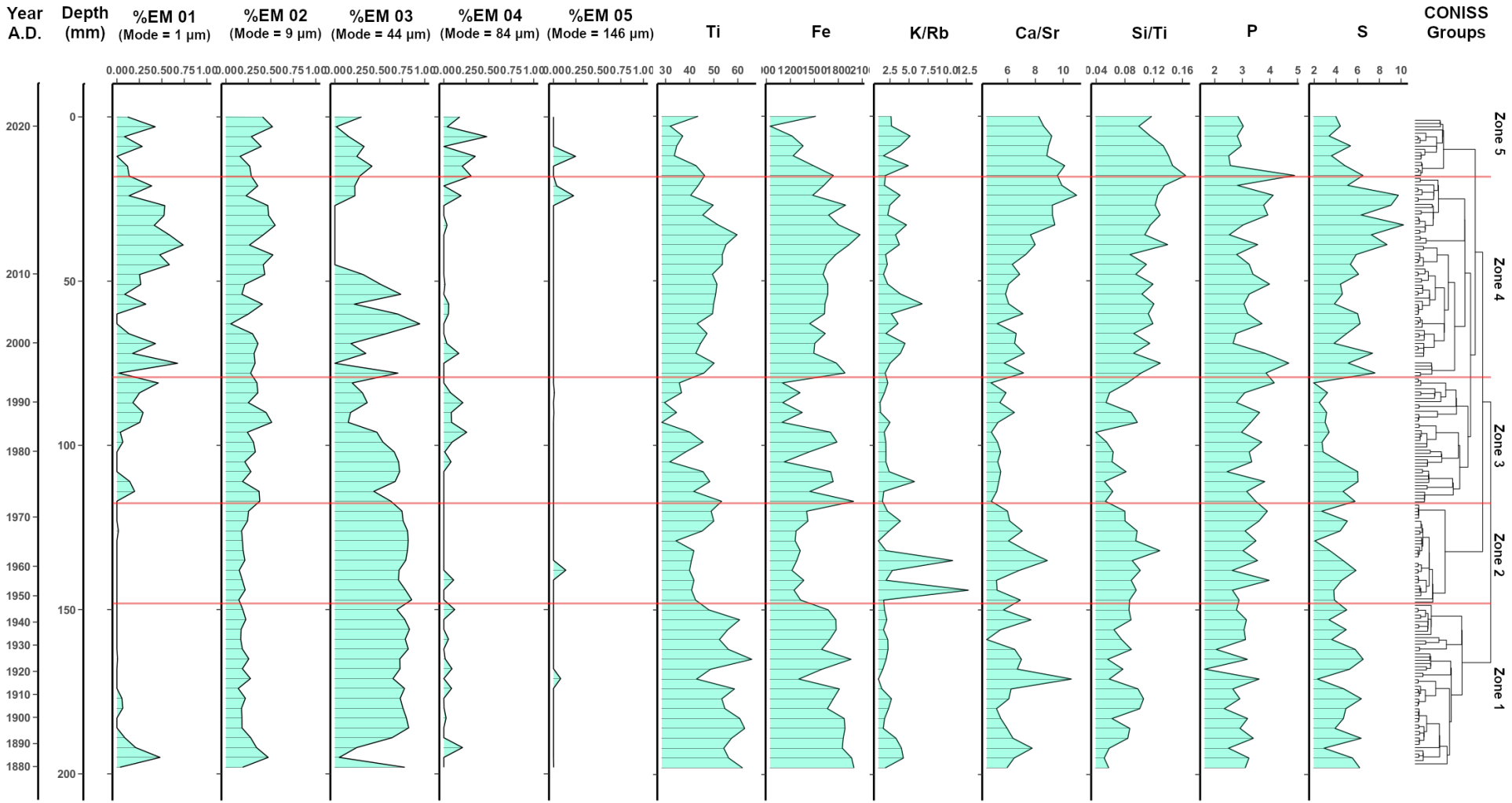

Figure 5. Down core EMMA and normalized ITRAX elemental profiles for Utikuma Lake in core BU1, plotted against depth and estimated age. The CONISS cluster dendrogram (right) indicates five zones, the boundaries of which are marked by horizontal red lines.

3.3. Time Series Analysis

3.3.1. ITRAX

Interannual oscillations with periods ranging from 1.5 to 8.0 years are common among both the productivity and runoff proxies (Figure 6). Interdecadal–multidecadal oscillations are also prevalent, though at lower (<95%) statistical significance. Each of Ti, Fe, and Ca/Sr exhibit a ~25+ year oscillation throughout the core. Similar ~30+ year oscillations are present from approximately 1950 onward for K/Rb, Si/Ti, and S (Figure 6).

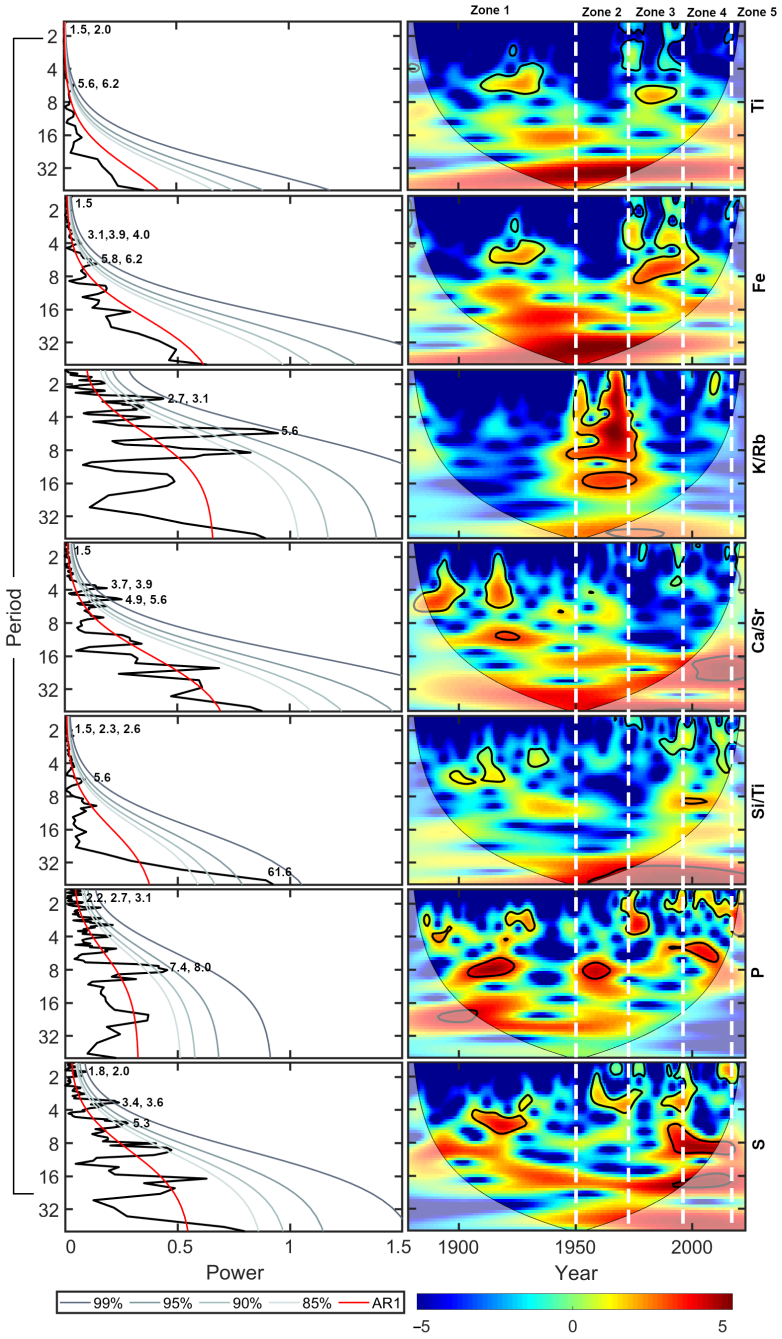

Figure 6. Spectral and wavelet time series analysis results of the normalized ITRAX elemental profiles for Utikuma Lake Core BU1. Red noise (AR1) and confidence levels are indicated on the spectrogram (**left**). Periodicities are indicated when the spectral power is statistically significant at 90%. Likewise, time-frequency areas of high spectral power, shown in red, which are statistically significant at 90% are indicated with black contouring on the CWT scalogram (**right**). CONISS boundaries (white dashed lines) overlay the wavelet scalograms.

The presence of many of the oscillatory components align with the CONISS zonations identified in Section 3.2 (Figure 5). For instance, the ~30+ year oscillation present in K/Rb, Si/Ti ratio, and S profiles appears after the Zone 1/2 transition. Interannual oscillations in K/Rb primarily exist in Zone 2, whereas similar oscillations in Ti and Fe are most prevalent in Zone 3 and during a segment of Zone 1 spanning ~1910–1940. While the productivity proxies (namely Si/Ti ratio and S) indicate several instances of interannual–interdecadal oscillations, these are most prevalent during Zone 4, after which their strength subsides (Figures 5 and 6).

3.3.2. EMMA

Oscillations in the 30–36-year range are present for EM01, EM02, EM03, and EM04 continuously throughout their records, though generally with lower significance in the mid-1900s (with the exception of EM04; Figure 7). Similar oscillations were present over the length of the ITRAX derived Fe, Ti, and Ca/Sr profiles (Figure 6). Interannual oscillations persist in clusters throughout each of the EM records, with a dearth of interannual oscillations occurring in EM01 from ~1930–1990, and in EM02 and EM03 from ~1930–1965. EM04, on the other hand, exhibits interannual oscillation throughout these intervals. For EM05, the EM record was too sparse to produce statistically robust results and was therefore omitted from this analysis (Figure 7).

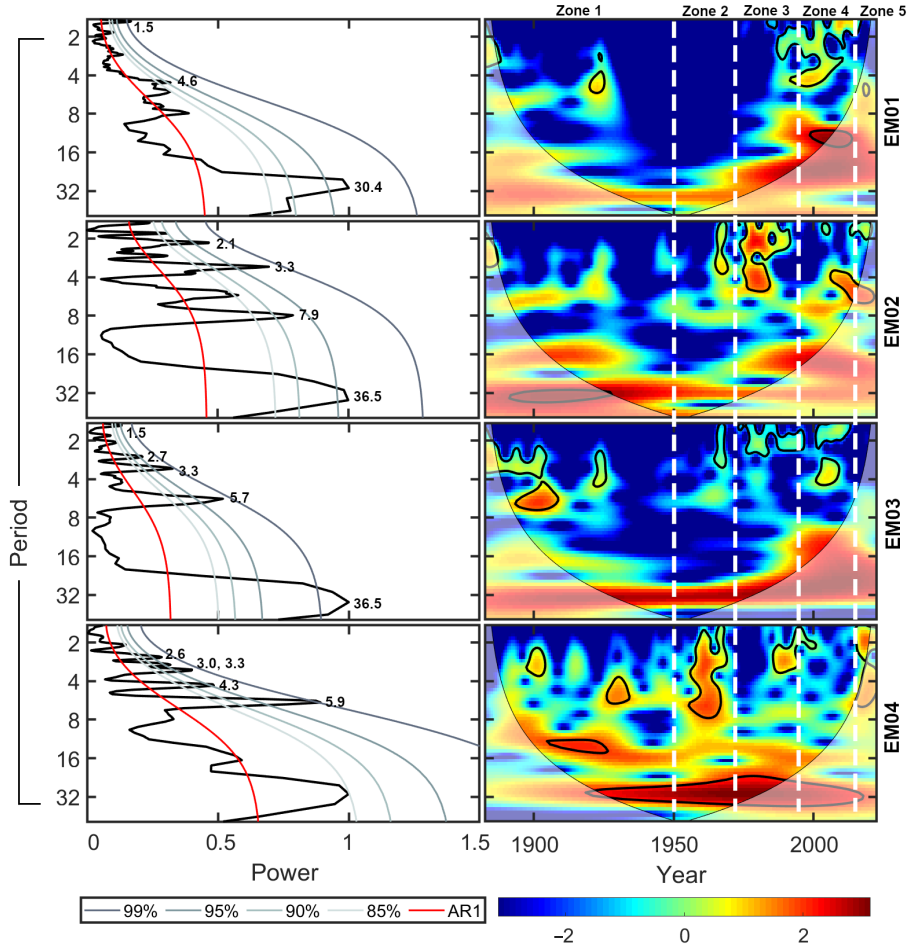

Figure 7. Spectral and wavelet analysis results for the five identified end members (EMs) identified in Utikuma Lake Core BU1. Oscillations above the 90% confidence level are labeled in the spectral time series results (**left**) and encircled in a solid black line in the wavelet time series analyses (**right**). CONISS boundaries (white dashed lines) overlay the wavelet scalograms.

4. Discussion

The EMMA and ITRAX-μXRF results from the late 19th–present core record can be interpreted together to shed light on sedimentary processes during the 20th century in Utikuma Lake. Grain-size EMs are often indicative of various environmental processes distinguished by sedimentary energy [11], and the ITRAX elemental ratios chosen are related to runoff or productivity [27,42]. These results are combined with precipitation data from Campsie, Alberta (∼200 km southeast of Utikuma Lake) to better constrain the cyclical behavior and environmental significance of the geological variables. This dataset was preferred over historical data from the closer Slave Lake because the record at the Campsie station is not only longer (1912–2013), but using Slave Lake's historical climate records would require combining data from multiple stations, which would still result in gaps in the record.

4.1. Spring Freshet

In northern Alberta, and other northern latitude regions, the most significant annual runoff event occurs during the spring thaw, when freshet water from the rapidly melting snowpack is released. This process results in the transport of coarser allochthonous material from the catchment into lakes and would be expected to feature very prominently in the sedimentary record of Utikuma Lake [11,43,44]. We suggest that the consistent presence of EM02, EM03, and the runoff proxies Ti and Fe throughout the core are indicative of spring freshet activity in Utikuma Lake. While Fe can be indicative of redox conditions, its similarity to the Ti record suggests a similar source for both elements (i.e., detrital/terriginous material; [22,28]). This interpretation raises two closely related questions: why would a single environmental process result in two distinct sedimentary EMs, and why is the spectral content broadly similar between the time series for these two EMs?

Previous research (e.g., [14,44–46]) has indicated that, in cold climates, two primary types of spring freshets occur; those associated with lower-energy and warmer weather, and those occurring during higher-energy and cooler weather. During colder springs, snowmelt is more prolonged, leading to an increase in meltwater in the snowpack. Ultimately, these cool spring conditions lead to a more sudden, intense delivery of coarser sediment to the system. Conversely, more moderate spring conditions result in gradual runoff, leading to a less intense influx of sediment to the lake [45]. Accordingly, we interpret the finer grain size distributions contributing to EM02 to be characteristic of a warmer spring, and the coarser EM03 to be characteristic of colder spring conditions.

The similarity in spectral frequencies between the time series for both EM02 and EM03 suggested a common oscillatory driver of these two regimes. Previous research suggests several cyclic teleconnections, including the Arctic Oscillation (AO), North Atlantic Oscillation (NAO), El Niño-Southern Oscillation (ENSO), and Pacific Decadal Oscillation (PDO). These teleconnections have previously all been associated with a variety of climatic patterns across North America, including impacts on temperature and snowpack [47–50].

Cross-wavelet transforms (XWTs) can be used to compare the CWTs of two signals to show the common components of both signals; in this case, the EM signals can each be compared to time series representing seasonal snowfall and a variety of known climatic oscillations [41]. For example, Figure 8 shows XWT results for EM02 and EM03 compared against each of the PDO, ENSO, AO, and NAO. These results indicate that the observed 30-year periodicity in both EMs is most prominently related the PDO. It is important to note that although the primary modes of the PDO are in the 15–25 and 50–70-year ranges [51,52], there is also an approximately 25–35-year PDO mode spanning the mid 20th century (Figure A1; [53–55]). When considering the sedimentary variables assessed, the 30-year periodicity is substantially continuous, and by comparison to the XWT results for

snowfall, it may be related to the influence of the AO and NAO after 25–35-year mode of the PDO receded. The 2–8-year periodicities, mostly observed toward the end of the 20th century in the EM02 and EM03 data, may be related to ENSO, which, like the PDO, is known to influence hydrologic systems in Western Canada [47,56,57]. Further still, the CONISS divisions observed here (Table 4) broadly align with regime shifts in the PDO in 1945/46, 1976/77, 1997/98, and mid-2010s [58–60], suggesting that the PDO is a substantial contributor to shifts in Utikuma Lake in the past century.

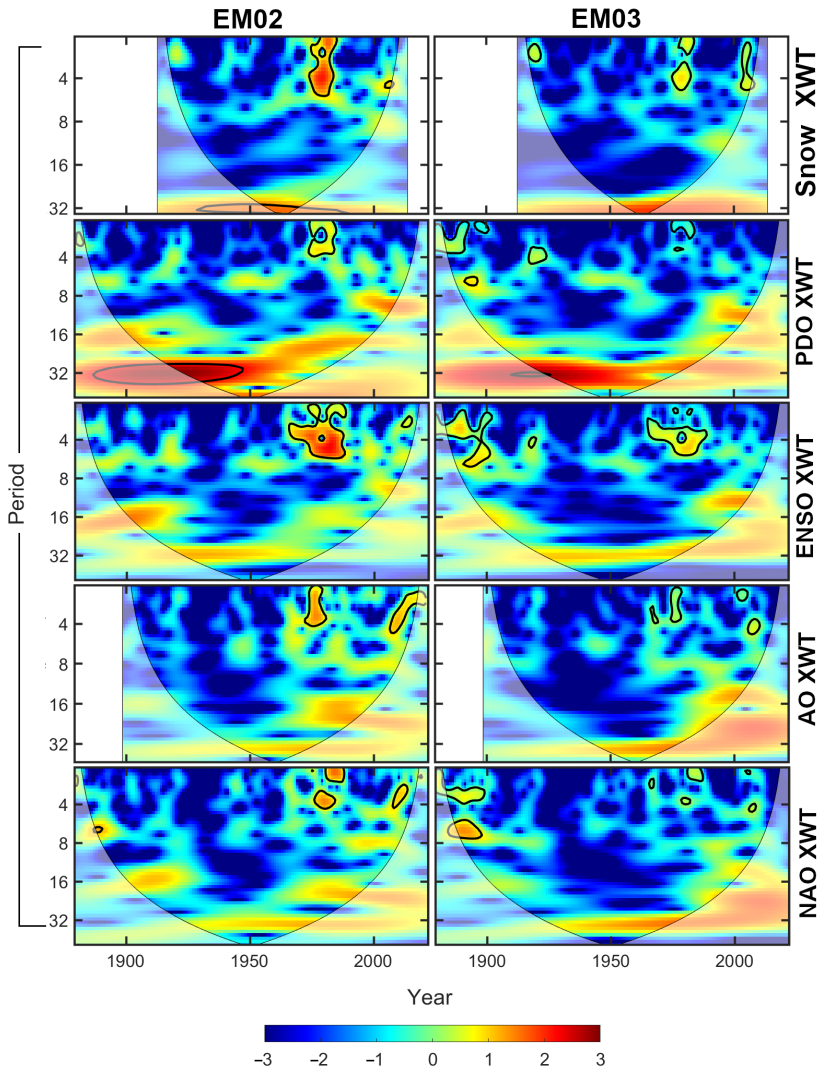

Figure 8. Cross wavelet transforms (XWTs) of EM02 and EM03 with annual snowfall total in Campsie, AB, and each of the PDO, ENSO, AO, and NAO. Oscillations above the 90% confidence level are encircled in a solid black line.

Finally, it is important to note that the deposition of either EM02 or EM03 in the Utikuma Lake core record depends on the phase of various teleconnections. While these teleconnections largely develop independently of each other and are characterized by their own ocean–atmosphere interactions, depending on their phase, they may either reinforce or suppress the effects of other teleconnections. Patterson et al. [61] analyzed 20th-century annually deposited varves from Effingham Inlet on the western coast of Vancouver Island. They found that the development of positive or negative phases of the PDO significantly influences the expression of both Schwabe solar cycles and ENSO in the sedimentary record, particularly before and after the Great PDO Regime shift of 1976–1977. In the Effingham Inlet record, ENSO displayed a varying period, differing during the cool PDO conditions

before 1976–1977 and the warm conditions after. The phase of the PDO similarly impacted the expression of 9–12-year Schwabe solar cycles, which dominated the Effingham Inlet record during the negative PDO conditions before 1976 and were suppressed during the subsequent positive phase.

4.2. Storms

Heavy rainfall events, whether from mid-latitude cyclones or thunderstorms, would be expected to influence the ecology and sedimentation of Utikuma Lake. We suggest that EM04, which occurs regularly in the sediment core but much less frequently compared to the spring freshet-derived EMs (EM02, EM03), is derived from major storm events (Figure 5). The coarser modal grain size of EM04 suggests higher energy rainfall events are required for the input of this EM. In contrast to storm sediments found in coastal or low-latitude locations (e.g., [62]), the rarity of EM04 can be attributed to the low incidence of very large storms in this continental high-latitude region. While the spectral signatures of EM02–EM04 all exhibit a similar ~30-year periodicity, EM04 stands out due to its more prominent 2–8-year periodicities (Figure 9). The two runoff proxies (K/Rb and Ca/Sr) and the three productivity proxies (P, S, and Si/Ti ratio) also exhibit more prominent 2–8 year periodicities, although the ~30-year periodicity is not as pronounced (Figure 9). The similarities in their spectral signatures suggest that these sedimentological variables (EM04, K/Rb, Ca/Sr, Si/Ti, P, and S) are interrelated. Since EM04 requires greater energy to deposit, it is possible that the sediment originates from a different source than the sediment from a spring freshet. This could explain the association of K/Rb and Ca/Sr with EM04, as opposed to the association of Fe and Ti with spring freshets. Winds and heavy rainfall associated with these large storms, unlike spring freshets, may have a greater influence on productivity as the sudden influx of sediment and increased mixing of the water column can disturb the lake ecosystem [63,64]. This could explain the similarity in spectral power between EM04 and the productivity proxies Si/Ti, P, and S.

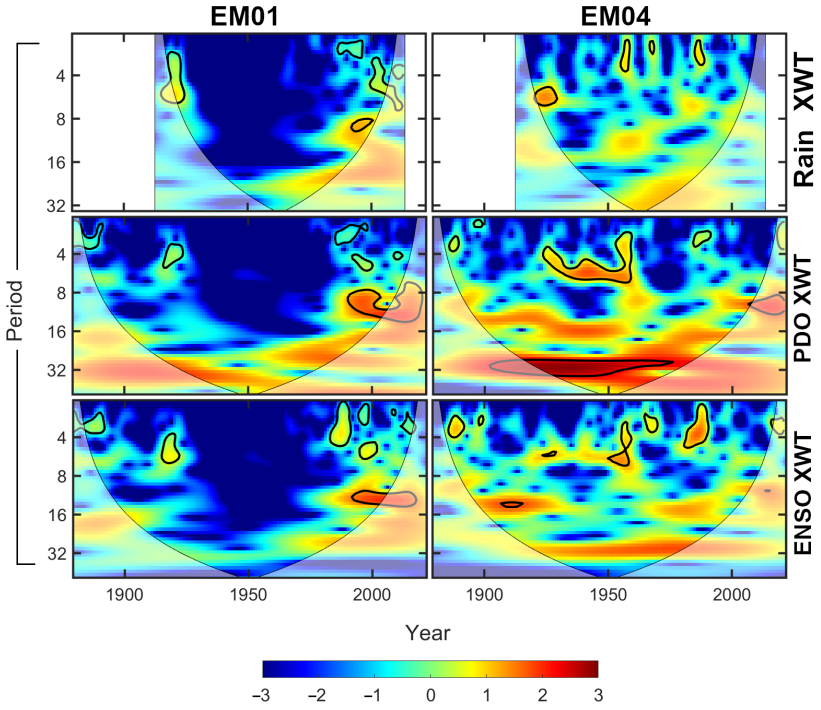

Figure 9. Cross wavelet transforms (XWTs) of EM01 and EM04 with annual rainfall total in Campsie, AB, and each of the PDO and ENSO. Oscillations above the 90% confidence level are encircled in a solid black line.

A similar exercise was performed for climatic data as was performed for the spring freshet above. XWTs between EM04 with PDO and ENSO time series are shown in Figure 9. The XWT analysis suggests that these 2–8-year periodicities are likely influenced by ENSO and PDO. The PDO-EM04 XWT also prominently features a common ~30-year periodicity.

In contrast to EM04, EM01, which is primarily composed of clay-sized particles with a less prominent coarse tail, is more characteristic of lower-energy inputs to the system, such as baseflow. Some researchers have attributed similarly defined EMs to the weathering of catchment soils, likely resulting from more moderate precipitation events [11,33,65]. As EM01 is not characterized by cyclic activity, it likely arises from processes outside of those responsible for EM04 and the related runoff and productivity proxies.

4.3. Anthropogenic Influence

Many of the patterns recognized in the ITRAX and EMMA stratigraphic datasets correspond with known settlement and land use changes within the Utikuma catchment through time. For instance we interpret the very coarse EM, EM05, primarily as a record of anthropogenic inputs. EM05 appears only briefly in the 1910s and 1960s, and for a more extended period in the late 2010s. The period in the late 2010s coincided with the construction of a new water treatment plant in adjacent Atikameg [66], which led to an influx of coarser sediments into the lake. The instances of this EM in the 1910s and 1960s likely coincided with other instances of significant land use change in the catchment.

CONISS cluster analysis revealed several clear breaks in both the ITRAX and EMMA records that correspond to distinctive paleolimnological phases in the history of Utikuma Lake (Figure 5). ITRAX analysis indicates that the lake, currently characterized as hyper-eutrophic [1], has experienced variable levels of eutrophication throughout its entire core record, which spans back to the late 19th century. This is characterized here by the primary productivity proxies S, P, and Si/Ti. Sulfur is found in relatively low concentrations in oligotrophic lake environments, but higher levels occur in nutrient-rich eutrophic locations characterized by significant concentrations of macrophytes, where natural biochemical sulfur cycling occurs [67]. Although P is a macronutrient essential for all forms of life, it is also the primary cause of eutrophication in lakes, particularly those subjected to point source pollution from sewage and agricultural runoff [68]. Excess P leads to eutrophication and associated algal blooms and macrophyte growth, which result in the depletion of oxygen levels in aquatic ecosystems [69]. Biogenic silica (SiO_2) serves as an indicator of diatom abundance and productivity in lacustrine sediments, as evidenced by the relative abundance of Si detected through ITRAX analysis [27,28]. The Si/Ti ratio is used to normalize Si content, ensuring that changes reflect diatomaceous sediment contributions rather than increased siliciclastic deposition from the catchment, making it a useful proxy for eutrophication [27,70,71].

In Utikuma Lake, the relative abundance of productivity proxies increased abruptly above already very high background levels starting in the mid-1990s (Figure 5). By approximately 2015–2017, concentrations reached their highest levels in the available late 19th century to present record. However, levels have trended to be progressively lower since 2018. Notably, throughout the entire stratigraphic record, changes in the relative abundance of these productivity indicators (P, S, Si/Ti) have mirrored similar changes in the relative abundance of Ti and Fe, which serve as proxies for precipitation-related runoff from the catchment [11,28].

The unprecedented and anomalously high levels of productivity proxies observed from the mid-1990s onward in Utikuma Lake may have been triggered by a well-documented extraordinary event. According to personal communications from the WLFN, including co-author Fabian Grey and WLFN Elders (pers. comm., 2024), the extraordinary increase in

productivity observed in the lake may be associated with two major incidents of sewage discharge. Following the establishment of a large new sewage plant and lagoon for the community of Atikameg, two smaller sewage lagoons were scheduled for decommissioning: one located on the shore of Mink Creek, which flows from Utikumasis Lake to Utikuma Lake, and the other situated on the eastern shore of Utikumasis Lake. In 1996, to remove the contents of these lagoons, the contractor simply breached the berm of the sewage lagoon on the shore of Utikumasis Lake, allowing the contents to flow freely into the lake and subsequently downstream into Utikuma Lake. The productivity proxy data for S, P, and the Si/Ti ratio indicate an immediate and dramatic spike in lake productivity following the 1996 sewage release (Figure 5). Utikuma Lake, which was already eutrophic, was pushed beyond a trophic tipping point resulting in the hypereutrophic conditions that are still present today. Subsequently, in 2004, the contents of the sewage lagoon on Mink Creek were similarly released, almost immediately reaching Utikuma Lake. This second release seems to not have had as dramatic an impact as the 1996 release, probably because the lake was already hypereutrophic.

The change in trophic state seems to have severely negatively impacted a commercial fishery that existed in Utikuma Lake. Following the initial 1996 sewage release there was an almost immediate decline in the spawning of whitefish from Utikuma Lake and Utikumasis Lake. Commercial fishing in Utikuma Lake came to an end in 2012 (co-author Fabian Grey and WLFN Elders, Pers. comm., 2024). To put the scale of destruction of this fishery in context, despite significant declines in the whitefish population after 1996 it still contributed 43.7% of the Alberta commercial whitefish catch in 2006 [72]. In 2018, during the last year of lake monitoring, it was observed that the current population of mature specimens of lake whitefish has significantly decreased and is unable to support a sustainable fishery [73,74]. Additionally, the high incidence of winter kill due to low under-ice oxygen levels, associated with the lake's hypereutrophic status, makes recovery of the fishery nearly impossible until eutrophication levels are reduced [73]. Co-author Dwayne Thunder assessed the whitefish population during the summer of 2023 by deploying multiple nets for 16 and 24 h intervals, respectively. No fish were captured during this assessment.

Although evidence strongly suggests that the sewage release starting in 1996 contributed significantly to Utikuma Lake's transition to hypereutrophic status, a simultaneous peak in Ti and Fe runoff proxies indicates that catchment disturbance may have also influenced the lake's change in trophic state (Figure 5). While the sewage discharge is likely the primary cause of the initial sharp increase in eutrophication levels, the effects of PDO and ENSO may have exacerbated the eutrophication (e.g., changes in temperature and/or precipitation regimes, seasonal ice cover, and wind patterns). This is indicated by the prominence of PDO and ENSO oscillations in productivity proxies and increased summer and fall rainfall toward the end of the 20th century and into the 21st century (Figure 6).

5. Conclusions

Through the implementation of paleolimnological techniques and various statistical analyses, we have demonstrated that both anthropogenic and climatic influences have caused variations in the limnological conditions of Utikuma Lake. The most significant change occurred in 1996, negatively impacting lake health, when productivity drastically increased. This is documented by a dramatic and rapid increase in P, S, and Si/Ti ratios beyond a trophic tipping point to hypereutrophy. This event coincided with the discharge from a decommissioned sewage lagoon upstream in nearby Utikumasis Lake. Climatic variability related to shifts in the influence of the Pacific Decadal Oscillation (PDO) and El Niño-Southern Oscillation (ENSO) toward higher summer and fall rainfall levels and/or more extreme rain events, as documented by runoff proxies (K/Rb, Ca/Sr), may have exac-

erbated the observed productivity shift. Evidence of extreme rainfall events in the summer and fall is also documented by the presence of the coarser-grained EM04 (mode = 84 μm). Numerous instances of discontinuous interannual spectral content are likely related to ENSO. Of particular interest is an interdecadal oscillation, likely related to the Pacific Decadal Oscillation (PDO), present in the EM time series but only in the summer rainfall time series. This suggests that the influence of thunderstorms, as opposed to mid-latitude cyclones, may be separately reflected in the spectral content of this EM.

The runoff and productivity proxies, EMMA, and a comparison to climatic data were used to constrain the effects of the spring freshet. This is reflected in two sedimentary EMs, EM02 (mode = 9 μm), and EM03 (mode = 44 μm), representing a common occurrence in cold climates where warmer (cooler) springs result in lower EM02 (higher, EM03) energy freshets. The spectral content of these two EM time series is similar and aligns with the spectral content of fall and winter snowfall time series, which show influences from the PDO, ENSO, AO, and NAO. These results confirm that cooler springs result in more sediment reworking, while the total amount of mobilized sediment is more highly influenced by the snowpack.

The very coarse EM05 (mode = 146 μm) appears only briefly in the 1910s and 1960s and for a more extended period in the late 2010s. This EM is interpreted as evidence of infrastructure construction in the catchment, such as the construction of a new water treatment plant in adjacent Atikameg in the late 2010s [66], which led to an influx of coarser sediments into the lake. The presence of this EM in the 1910s and 1960s likely coincided with other significant land-use changes in the catchment. In contrast, EM01 (mode = 1 μm) typifies very low-energy inputs into the lake system from the catchment, possibly related to smaller scale rainfall events.

Author Contributions: Conceptualization, R.T.P. and F.G.; methodology, R.T.P., C.R.W., C.W.P., E.G.R. and M.R.; software, C.R.W. and M.R.; validation, C.R.W.; formal analysis, C.R.W.; investigation, R.T.P., C.W.P., F.G., D.G., H.G. and D.T.; resources, R.T.P., C.W.P., F.G., D.G., H.G. and D.T.; data curation, C.R.W.; writing—original draft preparation, C.R.W. and M.R.; writing—review and editing, C.R.W., M.R., R.T.P., C.W.P., E.G.R. and F.G.; visualization, C.R.W. and M.R.; supervision, C.R.W. and R.T.P.; project administration, R.T.P.; funding acquisition, R.T.P. and F.G. All authors have read and agreed to the published version of the manuscript.

Funding: This project was carried out in collaboration, and with the financial support of Members of the White Fish Lake First Nation 459 and Solstice Environmental Management. The research was also supported by NSERC Discovery (#RGPIN05329) and NRCan Clean Technology (#CGP-17-0704) grants to RTP.

Data Availability Statement: The ITRAX-XRF, grain-size and derived EMMA data are available at [75]. Data for the climate oscillations used—PDO, AO, NAO, and ENSO—was obtained from [59,76–78], respectively.

Acknowledgments: Appreciation for direct support of the project in the field is made to Fabian Grey, Elder Dennis Grey and Elder Henry Grey and Dwayne Thunder (boat skipper) of White Fish Lake First Nation, and to Vera Moostoos, Erin Taylor, and Josh Wasyliw of Solstice Environmental Research. Additional thanks to Braden Gregory and Marin Netterfield for their assistance in the laboratory work.

Conflicts of Interest: The authors declare no conflicts of interest.

Abbreviations

The following abbreviations are used in this manuscript:

WLFN	Whitefish Lake First Nation
EMMA	End-Member Modeling Analysis
MTM	Multitaper Method

CWT	Continuous Wavelet Transform
XWT	Cross Wavelet Transform
PDO	Pacific Decadal Oscillation
NAO	North Atlantic Oscillation
AO	Arctic Oscillation
ENSO	El Niño Southern Oscillation

Appendix A

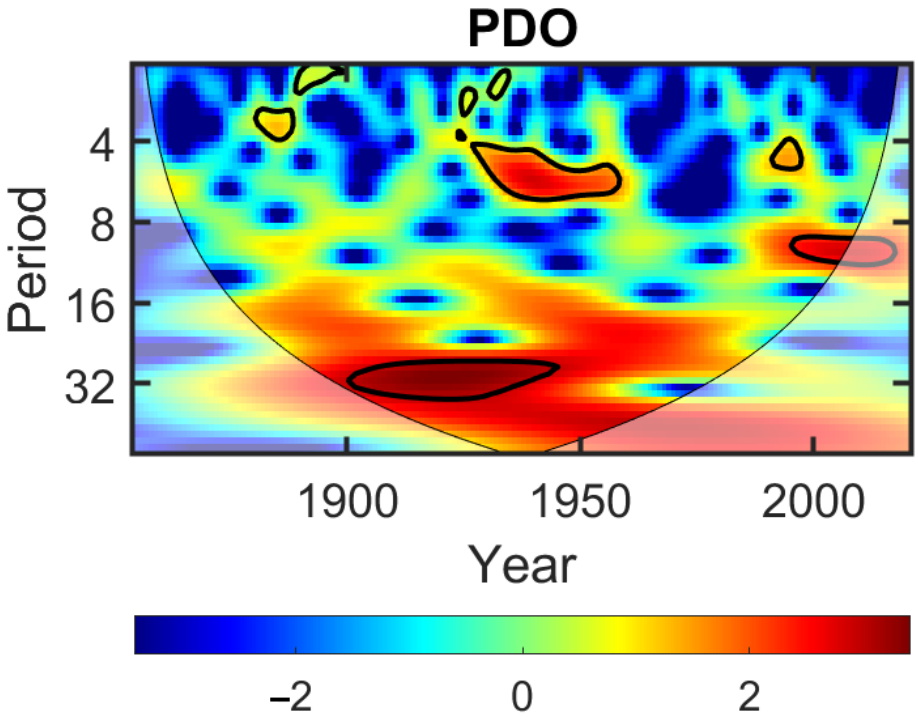

Figure A1. Continuous wavelet transform (CWT) of the Pacific Decadal Oscillation. Oscillations above the 90% confidence level are encircled in a solid black line.

References

1. CPP Environmental. *Utikuma Lake 2018 Monitoring Report*; CPP Environmental: Sherwood Park, AB, Canada, 2020.
2. Paerl, H.W.; Barnard, M.A. Mitigating the global expansion of harmful cyanobacterial blooms: Moving targets in a human-and climatically-altered world. *Harmful Algae* **2020**, *96*, 101845. [CrossRef] [PubMed]
3. Erratt, K.J.; Creed, I.F.; Lobb, D.A.; Smol, J.P.; Trick, C.G. Climate change amplifies the risk of potentially toxigenic cyanobacteria. *Glob. Change Biol.* **2023**, *29*, 5240–5249. [CrossRef]
4. Schindler, D.; Wolfe, A.P.; Vinebrooke, R.; Crowe, A.; Blais, J.M.; Miskimmin, B.; Freed, R.; Perren, B. The cultural eutrophication of Lac la Biche, Alberta, Canada: A paleoecological study. *Can. J. Fish. Aquat. Sci.* **2008**, *65*, 2211–2223. [CrossRef]
5. Schindler, D.W.; Hecky, R.E.; McCullough, G.K. The rapid eutrophication of Lake Winnipeg: Greening under global change. *J. Great Lakes Res.* **2012**, *38*, 6–13. [CrossRef]
6. Taranu, Z.E.; Gregory-Eaves, I.; Leavitt, P.R.; Bunting, L.; Buchaca, T.; Catalan, J.; Domaizon, I.; Guilizzoni, P.; Lami, A.; McGowan, S.; et al. Acceleration of cyanobacterial dominance in north temperate-subarctic lakes during the Anthropocene. *Ecol. Lett.* **2015**, *18*, 375–384. [CrossRef]
7. O'Neil, J.M.; Davis, T.W.; Burford, M.A.; Gobler, C.J. The rise of harmful cyanobacteria blooms: The potential roles of eutrophication and climate change. *Harmful Algae* **2012**, *14*, 313–334. [CrossRef]
8. Huisman, J.; Codd, G.A.; Paerl, H.W.; Ibelings, B.W.; Verspagen, J.M.; Visser, P.M. Cyanobacterial blooms. *Nat. Rev. Microbiol.* **2018**, *16*, 471–483. [CrossRef] [PubMed]
9. Munawar, M.; Fitzpatrick, M. Eutrophication in three Canadian Areas of Concern: Phytoplankton and major nutrient interactions. *Aquat. Ecosyst. Health Manag.* **2018**, *21*, 421–437. [CrossRef]
10. Gushulak, C.A.; Chegoonian, A.M.; Wolfe, J.; Gray, K.; Mezzini, S.; Wissel, B.; Hann, B.; Baulch, H.M.; Finlay, K.; Leavitt, P.R. Impacts of hydrologic management on the eutrophication of shallow lakes in an intensive agricultural landscape (Saskatchewan, Canada). *Freshwater Biol.* **2024**, *69*, 984–1000. [CrossRef]

11. Patterson, R.T.; Nasser, N.A.; Reinhardt, E.G.; Patterson, C.W.; Gregory, B.R.; Mazzella, V.; Roe, H.M.; Galloway, J.M. End-Member Mixing Analysis as a Tool for the Detection of Major Storms in Lake Sediment Records. *Paleoceanogr. Paleoclimatol.* **2022**, *37*, e2022PA004510. [CrossRef]
12. MacDonald, G.M.; Larsen, C.P.; Szeicz, J.M.; Moser, K.A. The reconstruction of boreal forest fire history from lake sediments: A comparison of charcoal, pollen, sedimentological, and geochemical indices. *Quat. Sci. Rev.* **1991**, *10*, 53–71. [CrossRef]
13. Shotbolt, L.A.; Thomas, A.D.; Hutchinson, S.M. The use of reservoir sediments as environmental archives of catchment inputs and atmospheric pollution. *Prog. Phys. Geogr.* **2005**, *29*, 337–361. [CrossRef]
14. Gammon, P.R.; Neville, L.A.; Patterson, R.T.; Savard, M.M.; Swindles, G.T. A log-normal spectral analysis of inorganic grain-size distributions from a Canadian boreal lake core: Towards refining depositional process proxy data from high latitude lakes. *Sedimentology* **2017**, *64*, 609–630. [CrossRef]
15. Mitchell, P.; Prepas, E.E. *Atlas of Alberta Lakes*; University of Alberta: Edmonton, AB, Canada, 1990.
16. Sass, G.; Creed, I. Characterizing hydrodynamics on boreal landscapes using archived synthetic aperture radar imagery. *Hydrol. Process. Int. J.* **2008**, *22*, 1687–1699. [CrossRef]
17. Natural Regions Committee. *Natural Regions and Subregions of Alberta*; Technical Report Pub. No. T/852; Downing, D.J., Pettapiece, W.W., Ed.; Government of Alberta: Edmonton, AB, Canada, 2006.
18. Environment and Natural Resources Canada. Canadian Climate Normals 1991–2020 (Slave Lake). 2024. Available online: https://climate.weather.gc.ca/climate_normals/index_e.html#1991 (accessed on 25 July 2024).
19. Patterson, R.T.; Nasser, N.A.; Tremblay, S.; Galloway, J.M. A portable extruder for accurate and precise high-resolution subsampling of unconsolidated sediment cores. *J. Paleolimnol.* **2022**, *67*, 183–189. [CrossRef]
20. Swarzenski, P.W. ^{210}Pb Dating. In *Encyclopedia of Scientific Dating Methods*; Rink, W.J., Thompson, J., Eds.; Springer: Dordrecht, The Netherlands, 2013; pp. 1–11. [CrossRef]
21. Gregory, B.R.; Reinhardt, E.G.; Macumber, A.L.; Nasser, N.A.; Patterson, R.T.; Kovacs, S.E.; Galloway, J.M. Sequential sample reservoirs for Itrax-XRF analysis of discrete samples. *J. Paleolimnol.* **2017**, *57*, 287–293. [CrossRef]
22. Croudace, I.W.; Rindby, A.; Rothwell, R.G. ITRAX: Description and evaluation of a new multi-function X-ray core scanner. *Geol. Soc. Lond. Spec. Publ.* **2006**, *267*, 51–63. [CrossRef]
23. Gregory, B.R.; Patterson, R.T.; Reinhardt, E.G.; Galloway, J.M.; Roe, H.M. An evaluation of methodologies for calibrating Itrax X-ray fluorescence counts with ICP-MS concentration data for discrete sediment samples. *Chem. Geol.* **2019**, *521*, 12–27. [CrossRef]
24. Löwemark, L.; Bloemsma, M.; Croudace, I.; Daly, J.S.; Edwards, R.J.; Francus, P.; Galloway, J.M.; Gregory, B.R.; Huang, J.J.S.; Jones, A.F.; et al. Practical guidelines and recent advances in the Itrax XRF core-scanning procedure. *Quat. Int.* **2019**, *514*, 16–29. [CrossRef]
25. Thomson, J.; Croudace, I.; Rothwell, R. A geochemical application of the ITRAX scanner to a sediment core containing eastern Mediterranean sapropel units. *Geol. Soc. Lond. Spec. Publ.* **2006**, *267*, 65–77. [CrossRef]
26. Chagué-Goff, C.; Chan, J.C.H.; Goff, J.; Gadd, P. Late Holocene record of environmental changes, cyclones and tsunamis in a coastal lake, Mangaia, Cook Islands. *Isl. Arc* **2016**, *25*, 333–349. [CrossRef]
27. McNeill-Jewer, C.A.; Reinhardt, E.G.; Collins, S.; Kovacs, S.; Chan, W.M.; Devos, F.; LeMaillot, C. The effect of seasonal rainfall on nutrient input and biological productivity in the Yax Chen cave system (Ox Bel Ha), Mexico, and implications for μXRF core studies of paleohydrology. *Palaeogeogr. Palaeoclimatol. Palaeoecol.* **2019**, *534*, 109289. [CrossRef]
28. Rothwell, R.G.; Croudace, I.W. Twenty Years of XRF Core Scanning Marine Sediments: What Do Geochemical Proxies Tell Us? In *Micro-XRF Studies of Sediment Cores: Applications of a Non-Destructive Tool for the Environmental Sciences*; Croudace, I.W., Rothwell, R.G., Eds.; Springer: Dordrecht, The Netherlands, 2015; pp. 25–102. [CrossRef]
29. Murray, M.R. Is laser particle size determination possible for carbonate-rich lake sediments? *J. Paleolimnol.* **2002**, *27*, 173–183. [CrossRef]
30. van Hengstum, P.; Reinhardt, E.; Boyce, J.; Clark, C. Changing sedimentation patterns due to historical land-use change in Frenchman's Bay, Pickering, Canada: Evidence from high-resolution textural analysis. *J. Paleolimnol.* **2007**, *37*, 603–618. [CrossRef]
31. R Core Team. *R: A Language and Environment for Statistical Computing*; R Foundation for Statistical Computing: Vienna, Austria, 2022.
32. Dietze, E.; Dietze, M. Grain-size distribution unmixing using the R package EMMAgeo. *E G Quat. Sci. J.* **2019**, *68*, 29–46.
33. Dietze, E.; Hartmann, K.; Diekmann, B.; IJmker, J.; Lehmkuhl, F.; Opitz, S.; Stauch, G.; Wünnemann, B.; Borchers, A. An end-member algorithm for deciphering modern detrital processes from lake sediments of Lake Donggi Cona, NE Tibetan Plateau, China. *Sediment. Geol.* **2012**, *243–244*, 169–180. [CrossRef]
34. Grimm, E.C. CONISS: A FORTRAN 77 program for stratigraphically constrained cluster analysis by the method of incremental sum of squares. *Comput. Geosci.* **1987**, *13*, 13–35. [CrossRef]
35. Juggins, S. Rioja: Analysis of Quaternary Science Data (Version 1.0-5). 2022. Available online: https://cran.r-project.org/package=rioja (accessed on 19 December 2024).

36. Chen, Y.; Tong, M.S.; Mittra, R. Efficient and accurate finite-difference time-domain analysis of resonant structures using the Blackman–Harris window function. *Microw. Opt. Technol. Lett.* **1997**, *15*, 389–392. [CrossRef]
37. Thomson, D.J. Spectrum estimation and harmonic analysis. *Proc. IEEE* **1982**, *70*, 1055–1096. [CrossRef]
38. Schulz, M.; Mudelsee, M. REDFIT: Estimating red-noise spectra directly from unevenly spaced paleoclimatic time series. *Comput. Geosci.* **2002**, *28*, 421–426. [CrossRef]
39. Husson, D.; Thibault, N.; Galbrun, B.; Gardin, S.; Minoletti, F.; Sageman, B.; Huret, E. Lower Maastrichtian cyclostratigraphy of the Bidart section (Basque Country, SW France): A remarkable record of precessional forcing. *Palaeogeogr. Palaeoclimatol. Palaeoecol.* **2014**, *395*, 176–197. [CrossRef]
40. Torrence, C.; Compo, G.P. A practical guide to wavelet analysis. *Bull. Am. Meteorol. Soc.* **1998**, *79*, 61–78. [CrossRef]
41. Grinsted, A.; Moore, J.C.; Jevrejeva, S. Application of the cross wavelet transform and wavelet coherence to geophysical time series. *Nonlinear Process. Geophys.* **2004**, *11*, 561–566. [CrossRef]
42. Gushulak, C.A.; Reinhardt, E.G.; Cumming, B.F. Climate driven declines in terrestrial input over the middle and late Holocene of perched boreal lakes in northeast Ontario (Canada) and teleconnections to the North Atlantic. *Quat. Sci. Rev.* **2021**, *265*, 107056. [CrossRef]
43. Spence, C.; Woo, M.K. Hydrology of the northwestern subarctic Canadian Shield. In *Cold Region Atmospheric and Hydrologic Studies. The Mackenzie GEWEX Experience: Volume 2: Hydrologic Processes*; Springer: Berlin/Heidelberg, Germany, 2008; pp. 235–256.
44. Macumber, A.L.; Patterson, R.T.; Galloway, J.M.; Falck, H.; Swindles, G.T. Reconstruction of Holocene hydroclimatic variability in subarctic treeline lakes using lake sediment grain-size end-members. *Holocene* **2018**, *28*, 845–857. [CrossRef]
45. Cockburn, J.M.; Lamoureux, S.F. Hydroclimate controls over seasonal sediment yield in two adjacent High Arctic watersheds. *Hydrol. Process. Int. J.* **2008**, *22*, 2013–2027. [CrossRef]
46. Shi, D. Late Holocene Paleoclimate Reconstruction in Debauchery Bay, Northwest Territories Canada Using Particle Size Analysis and Geochemical Proxies. Master's Thesis, Carleton University, Ottawa, ON, USA, 2024.
47. Whitfield, P.H.; Moore, R.; Fleming, S.W.; Zawadzki, A. Pacific decadal oscillation and the hydroclimatology of western Canada—Review and prospects. *Can. Water Resour. J.* **2010**, *35*, 1–28. [CrossRef]
48. Newton, B.W.; Prowse, T.D.; Bonsal, B.R. Evaluating the distribution of water resources in western Canada using synoptic climatology and selected teleconnections. Part 1: Winter season. *Hydrol. Process.* **2014**, *28*, 4219–4234. [CrossRef]
49. Bevington, A.R.; Gleason, H.E.; Foord, V.N.; Floyd, W.C.; Griesbauer, H.P. Regional influence of ocean–atmosphere teleconnections on the timing and duration of MODIS-derived snow cover in British Columbia, Canada. *Cryosphere* **2019**, *13*, 2693–2712. [CrossRef]
50. RahimiMovaghar, M.; Fereshtehpour, M.; Najafi, M.R. Spatiotemporal pattern of successive hydro-hazards and the influence of low-frequency variability modes over Canada. *J. Hydrol.* **2024**, *634*, 131057. [CrossRef]
51. Mantua, N.J.; Hare, S.R. The Pacific decadal oscillation. *J. Oceanogr.* **2002**, *58*, 35–44. [CrossRef]
52. MacDonald, G.M.; Case, R.A. Variations in the Pacific Decadal Oscillation over the past millennium. *Geophys. Res. Lett.* **2005**, *32*, L08703. [CrossRef]
53. Beebee, R.A.; Manga, M. Variation in the Relationship Between Snowmelt Runoff in Oregon and ENSO and PDO. *J. Am. Water Resour. Assoc.* **2004**, *40*, 1011–1024. [CrossRef]
54. Ma, L.; Yin, Z. Possible solar modulation of pacific decadal oscillation. *Sol. Syst. Res.* **2017**, *51*, 417–421. [CrossRef]
55. Tamaddun, K.A.; Kalra, A.; Ahmad, S. Wavelet analyses of western US streamflow with ENSO and PDO. *J. Water Clim. Chang.* **2017**, *8*, 26–39. [CrossRef]
56. Gurrapu, S.; St-Jacques, J.M.; Sauchyn, D.J.; Hodder, K.R. The influence of the Pacific Decadal Oscillation on annual floods in the rivers of Western Canada. *J. Am. Water Resour. Assoc.* **2016**, *52*, 1031–1045. [CrossRef]
57. Nalley, D.; Adamowski, J.; Biswas, A.; Gharabaghi, B.; Hu, W. A multiscale and multivariate analysis of precipitation and streamflow variability in relation to ENSO, NAO and PDO. *J. Hydrol.* **2019**, *574*, 288–307. [CrossRef]
58. Deser, C.; Phillips, A.S.; Hurrell, J.W. Pacific interdecadal climate variability: Linkages between the tropics and the North Pacific during boreal winter since 1900. *J. Clim.* **2004**, *17*, 3109–3124. [CrossRef]
59. Deser, C.; Trenberth, K.E.; National Center for Atmospheric Research Staff (NCAR). (Eds.) The Climate Data Guide: Pacific Decadal Oscillation (PDO): Definition and Indices. 2022. Available online: https://climatedataguide.ucar.edu/climate-data/pacific-decadal-oscillation-pdo-definition-and-indices (accessed on 30 July 2023).
60. Xiao, D.; Ren, H.L. A regime shift in North Pacific annual mean sea surface temperature in 2013/14. *Front. Earth Sci.* **2023**, *10*, 987349. [CrossRef]
61. Patterson, R.T.; Chang, A.S.; Prokoph, A.; Roe, H.M.; Swindles, G.T. Influence of the Pacific Decadal Oscillation, El Niño-Southern Oscillation and solar forcing on climate and primary productivity changes in the northeast Pacific. *Quat. Int.* **2013**, *310*, 124–139. [CrossRef]
62. Czajkowski, J.; Simmons, K.; Sutter, D. An analysis of coastal and inland fatalities in landfalling US hurricanes. *Nat. Hazards* **2011**, *59*, 1513–1531. [CrossRef]

63. Stockwell, J.D.; Doubek, J.P.; Adrian, R.; Anneville, O.; Carey, C.C.; Carvalho, L.; De Senerpont Domis, L.N.; Dur, G.; Frassl, M.A.; Grossart, H.P.; et al. Storm impacts on phytoplankton community dynamics in lakes. *Glob. Change Biol.* **2020**, *26*, 2756–2784. [CrossRef]
64. Hampton, S.E.; Sharma, S.; Brousil, M.R.; Filazzola, A. Winter and summer storms modify chlorophyll relationships with nutrients in seasonally ice-covered lakes. *Ecosphere* **2022**, *13*, e4272. [CrossRef]
65. Xiao, J.; Chang, Z.; Fan, J.; Zhou, L.; Zhai, D.; Wen, R.; Qin, X. The link between grain-size components and depositional processes in a modern clastic lake. *Sedimentology* **2012**, *59*, 1050–1062. [CrossRef]
66. Froese, R. *Better Water Coming to Atikameg*; South Peace News: High Prairie, AB, Canada, 2016.
67. Holmer, M.; Storkholm, P. Sulphate reduction and sulphur cycling in lake sediments: A review. *Freshw. Biol.* **2001**, *46*, 431–451. [CrossRef]
68. Kerekes, J.J.; Blouin, A.C.; Beauchamp, S.T. Trophic response to phosphorus in acidic and non-acidic lakes in Nova Scotia, Canada. *Hydrobiologia* **1990**, *191*, 105–110. [CrossRef]
69. Correll, D.L. The role of phosphorus in the eutrophication of receiving waters: A review. *J. Environ. Qual.* **1998**, *27*, 261–266. [CrossRef]
70. Johnson, T.C.; Brown, E.T.; McManus, J.; Barry, S.; Barker, P.; Gasse, F. A high-resolution paleoclimate record spanning the past 25,000 years in southern East Africa. *Science* **2002**, *296*, 113–132. [CrossRef]
71. Johnson, T.C.; Brown, E.T.; Shi, J. Biogenic silica deposition in Lake Malawi, East Africa over the past 150,000 years. *Palaeogeogr. Palaeoclimatol. Palaeoecol.* **2011**, *303*, 103–109. [CrossRef]
72. Department of Fisheries and Oceans. *Annual Summary of Fish Harvesting Activities*; Department of Fisheries and Oceans: Winnipeg, MB, Canada, 2010; Volume 25, Xiii + 88p.
73. Government of Alberta. *Utikumasis Lake Fisheries Management Objectives*; Technical Report; Government of Alberta: Edmonton, AB, Canada, 2018.
74. Government of Alberta. *Utikuma Lake FIN Summary*; Technical Report; Government of Alberta: Edmonton, AB, Canada, 2019.
75. Walsh, C.R.; Patterson, R.T.; Ralchenko, M.; Patterson, C.W.; Reinhardt, E.G. *A 140-Year Paleolimnological Record of Climatically and Anthropogenically Driven Eutrophication in Utikuma Lake, Alberta, Canada*; [Dataset], Dryad; Carleton University: Ottawa, ON, Canada, 2024. [CrossRef]
76. Hurrell, J.; National Center for Atmospheric Research Staff (NCAR). (Eds.) The Climate Data Guide: Hurrell North Atlantic Oscillation (NAO) Index (Station-Based). 2022. Available online: https://climatedataguide.ucar.edu/climate-data/hurrell-north-atlantic-oscillation-nao-index-station-based (accessed on 30 July 2023).
77. National Center for Atmospheric Research Staff (NCAR). (Ed.) The Climate Data Guide: Hurrell Wintertime SLP-Based Northern Annular Mode (NAM) Index. 2022. Available online: https://climatedataguide.ucar.edu/climate-data/hurrell-wintertime-slp-based-northern-annular-mode-nam-index (accessed on 30 July 2023).
78. Trenberth, K.E.; National Center for Atmospheric Research Staff (NCAR). (Eds.) The Climate Data Guide: Nino SST Indices (Nino 1+2, 3, 3.4, 4; ONI and TNI). 2022. Available online: https://climatedataguide.ucar.edu/climate-data/nino-sst-indices-nino-12-3-34-4-oni-and-tni (accessed on 30 July 2023).